International Journal of Geo-Information

MDPI

Article

3-D Morphological Change Analysis of a Beach with Seagrass Berm Using a Terrestrial Laser Scanner

Hugo Corbí [1,*], Adrian Riquelme [2,*,†], Clara Megías-Baños [3] and Antonio Abellan [4]

1 Department of Earth Sciences and the Environment, University of Alicante, 03690 Alicante, Spain
2 Department of Civil Engineering, University of Alicante, 03690 Alicante, Spain
3 Marine Science Degree, University of Alicante, 03690 Alicante, Spain; claramega@gmail.com
4 School of Earth and Environment, University of Leeds, Leeds LS2 9JT, UK; A.Abellan@leeds.ac.uk
* Correspondence: hugo.corbi@ua.es (H.C.); ariquelme@ua.es (A.R.); Tel.: +34-96590-3400 (ext. 1215)
† Co-Fist Author.

Received: 4 May 2018; Accepted: 18 June 2018; Published: 21 June 2018

Abstract: Along many Mediterranean coasts, the detached seagrass material of *Posidonia oceanica* creates seagrass berms that control the structure and morphodynamics of sandy beaches. Here, we show how Terrestrial Laser Scanner remote sensing data allows analyzing the 3-D morphologic change of beaches where this characteristic geomorphic structure is present. We propose a methodology for estimating accretion/erosion (almost -200 m^3 in our study) by considering the sand dominated and seagrass berms as two independent elements. For this purpose, two different sampling dates (named scenarios A and B, before and after an erosive heavy storms period, respectively) recorded in a microtidal pocket-beach (300 m^2) with these characteristic geomorphic structures have been modeled in 3-D. The present approach constitutes a cost-efficient, accurate, and quick tool to survey the sand volume in natural and artificial replenished beaches. The innovative approach, which can be considered as a conceptual and methodological starting point, can be useful to examine long-term and high-precision data sets in future studies of the morphodynamic evolution of these characteristic Mediterranean beaches.

Keywords: terrestrial laser scanner; coastal geomorphology; remote sensing; 3-D modeling; western Mediterranean

1. Introduction

The morphodynamics of sandy beaches depend on a set of variables, such as sediment granulometry, breaker wave climate (wave height and period), tide range, and major topographic features (beach slope and embayment shape) [1]. The morphology and water circulation of a beach can be influenced by detached seaweed and seagrasses, which can be accumulated, forming patches and wrack banks on the beach [2–6]. These accumulations of this detached material are referred as seagrass berms [7], although they have also been named in the scientific literature as beach-cast, beach wrack, or beach strand [8], or "*banquettes*" according to the French naming [9–11].

The endemic seagrass *Posidonia oceanica* (L.) Delile forms extensive and highly productive meadows, which predetermine the dynamics and ecology of the coastal system along many Mediterranean coasts [12–14]. Indeed, the seagrass detached material of this plant shape characteristics of beach-cast accumulations around the Mediterranean coast [13,15,16]. The seagrass berms are more intensively accumulated when *P. oceanica* loses the leaves in early autumn [17], coincident with an increase of the wind strength [18]. As a result, the maximum heights of the seagrass berms are reached because of severe storms in winter time [15]. Such beach-cast accumulations create berm structures along the coast with heights ranging from a few centimetres to several meters and with heterogeneous spatial distribution [11].

The role of *Posidonia oceanica* seagrass berms in the protection of sandy beaches is controversial; while some authors claimed that the seagrass berms have a marginal role in beach protection [16], some other authors pointed out that these accumulations help to dissipate the wave energy during winter storms [19], and that their removal for aesthetic reasons could have sedimentological, geomorphological, and ecological implications on the coastal morphodynamic system [13]. From a beach management perspective, long-term and high-precision time series, which can be developed using accurate 3-D geomorphological models, are essential to establish the morphodynamic evolution of beaches by integrating the seagrass berm as a key element.

3-D remote sensing techniques, such as Light Detection and Ranging (LiDAR) and digital photogrammetry, allowing the acquisition of millions of 3-D points at different periods of time have been applied to the investigation of coastal environments [20], together with other applications in archaeology [21], cultural heritage [22], ecology [23], geomatics [24], or rock mechanics [25], among other disciplines. Indeed, these techniques allow for the obtaining of accurate maps or Digital Elevation Models (DEM) of shoreline positions [26], and analyze morphodynamics and volumetric changes in both dunes [27–30] and beach systems [31,32]. Furthermore, some studies use LiDAR remote sensing to map the *P. oceanica* meadows [33], or to analyse the trend of the beach morphology with seagrass berms [34,35].

This paper focuses on examining the three-dimensional model provided by a Terrestrial Laser Scanner (TLS) of a beach with seagrass berms, which can be useful for future studies to examine the morphodynamic evolution of seagrass berms. Future investigations of our research team with data collected frequently will be adopted as a starting point using the methodology proposed here. We propose a straightforward and accurate methodology to estimate the sand volumetric changes. For this purpose, a western Mediterranean enclosed beach of small dimensions (Cala Quarter 1, Alicante, SE Spain), where a seagrass berm is the typical geomorphological feature is chosen. The application in future long-term series studies of the methodology proposed here, which permits to evaluate the beach morphological changes, takes on a special importance in the future management of a coastal area, where most of the beaches are artificially replenished due to shoreline erosion as a consequence of natural and human-induced causes.

2. Materials and Methods

2.1. Study Area

The studied beach, denominated Cala Quarter 1 (CC1 hereafter), is located to the east of the Santa Pola cape (province of Alicante, SE Spain) (Figure 1). For the purpose of this investigation, the studied beach was not subject to cleaning operations from September of 2016 to June of 2017, including the removal and dump of beach-cast litter accumulations. Contrarily, the rest of the beaches of the area were regularly cleaned for aesthetic reasons.

The CC1 beach, with a trapezoidal-like shape, currently covers an area of 300 m^2 and a maximum length and width of 60 m and 30 m respectively. The beach is open to the east, and has been artificially replenished in the past, especially since the 90s decade. The shore platform presents a small angle of inclination (1–2%), and has a *P. oceanica* meadow close to the beach [36]. The potential erosive action occurs during periods of torrential rain, where the runoff water deriving from the close gullies could erode the beach. Particularly, in the autumn season, this area is subjected to storms and strong winds of Levante (component ENE), which usually coincide with extreme events [37]. The range of astronomical tides on the shores of Alicante is estimated to be between 8 cm and 10 cm, but occasionally the meteorological tides can play an important role in coastal erosion. Waves can reach up to 4.5 m in height in the area with significant erosional consequences on the shoreline [38] when strong easterly winds during autumn and winter run into high astronomical and meteorological tides.

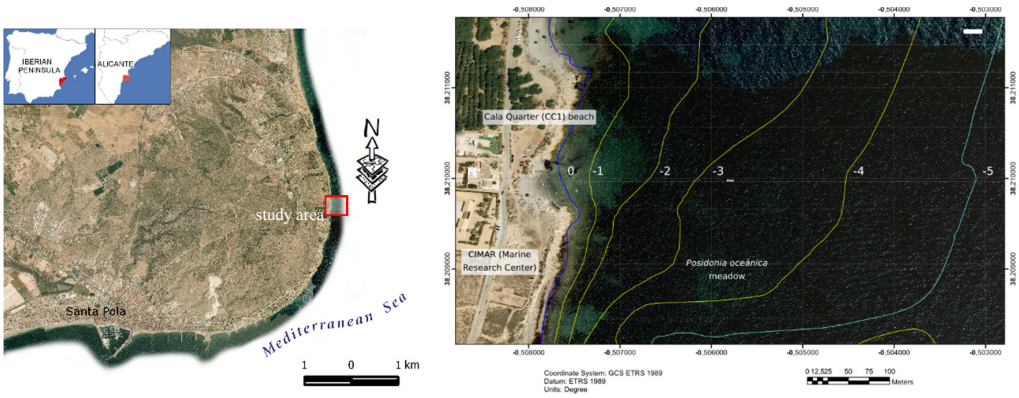

Figure 1. Geographical location of the studied beach in the context of the western Mediterranean. The figure on the left was prepared by Francisco Asensio-Montesinos.

Two different scenarios were analysed in this study on different sampling dates (Figures 2 and 3): 24 November 2016 (Scenario A), and 22 March 2017 (Scenario B). The second scenario represents the beach geometry after winter, when four storm events were recorded in study area one (5–20 December 2016; 17–23 January 2017; 11–13 February 2017; and 11–14 March 2017). All the storm intervals present east and north-eastern dominant winds (data from the nearby Alicante airport meteorological station, just 9 kilometres from the studied beach; data from AEMET). Note that both sampling dates present the same tidal coefficient, so they can be compared in terms of sea level.

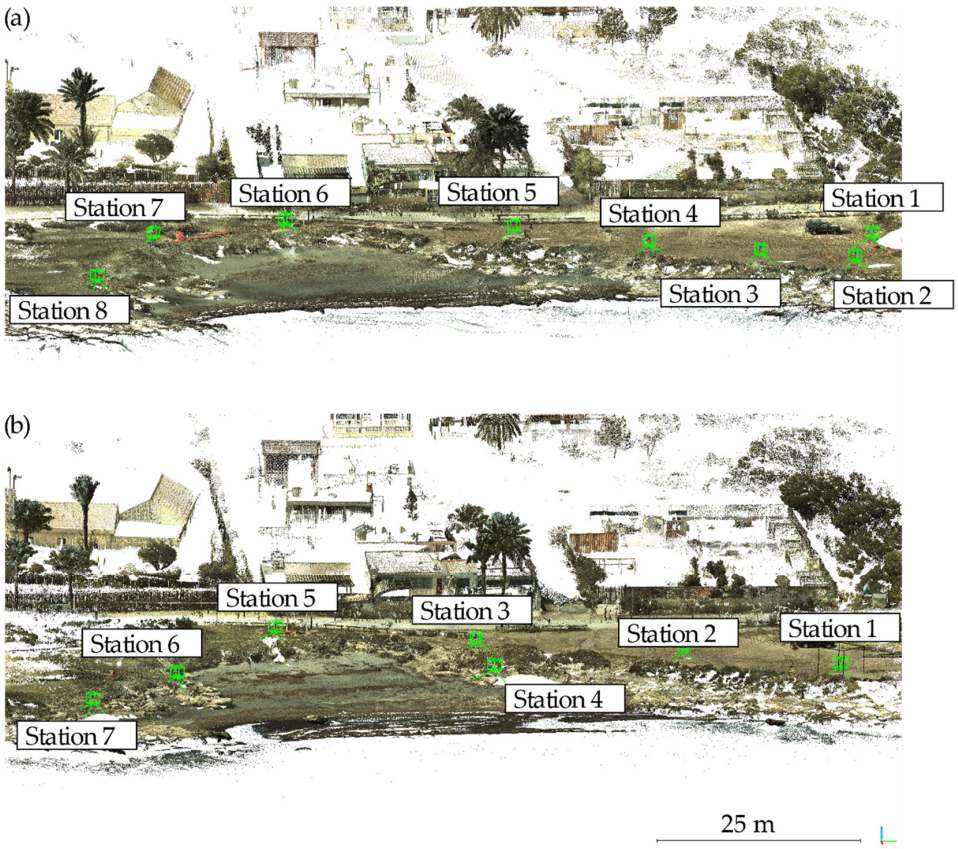

Figure 2. (**a**) 3-D point cloud of the scenario/sampling date A (24 November 2016) and location of the scan stations; (**b**) 3-D point cloud of the scenario/sampling date B (22 March 2017) and location of the scan stations.

2.2. Data Acquisition

The 3-D geometry of the study area was investigated using a TLS instrument that was able to capture both the geometry and the strength of the backscattered signal for each measured point [39]. The device (Leica ScanStation C10), allowed for capturing the 3-D coordinates and the intensity of millions of points on the visible surface, and the colour of the scanned points through the capture of photos during the scanning. The angular accuracy of this instrument is 12", the distance accuracy is 4 mm, and the noise is 2 mm at 50 m [40].

The area of interest was captured for each scenario with a spherical scan strategy; several stations were needed in order to reduce the presence of shadow areas on the 3-D model (Figure 2, Stations 8 and 7, respectively). Each dataset was captured in a local reference system, and they were subsequently registered in a common reference system using a Euclidean transformation, i.e., by allowing a rigid rotation and translation of each of the point clouds. This process could be conducted using different strategies, the most common of which being the use of targets or the application of the Iterative Closest Point algorithm (ICP) [41]. Another strategy was the use of targets of spheres, which accurately provided the coordinates of certain control points in the local reference system that are common for all scans. Then, the rigid transformation matrix was calculated in a simple manner. As the used TLS was a Leica C10 model, all scan stations were levelled so the rigid transformation only required an X, Y, and Z translation, and an OZ axis rotation. Additionally, photographs acquired from an Unmanned Aerial Vehicle (UAV) (DJI Phantom 3 Professional) were acquired in both scenarios for future works. These photos enabled the application the Structure-from-Motion (SfM) technique, which enabled the generation of 3-D point clouds. Although the use of this technique requires caution [42], this technique may also provide a dataset to apply to the presented methodology.

To register different scan stations, three High-Definition Surveying (HDS) Targets were distributed around the area of interest and were scanned, along with the area under investigation. The extraction of the coordinates' centres for each of the targets enabled the calculation of the rigid transformation matrix through a least square method, and the acquired point clouds were registered and merged into a local reference system. Then, the two scenarios were registered into the same reference system using the surrounding buildings as 'stable' areas, enabling the registration of the merged point clouds. This, and the aforementioned processes, were conducted thought the software Cyclone v9.1 [43].

The final step consisted of the alignment of the two scenarios into a global system by using a three-dimensional point cloud (3DPC) scanned in 2009 by an Aerial Laser Scanner (ALS) system under the Plan Nacional de Ortofoto Aérea Project (PNOA), which was available on the Instituto Geográfico Nacional (IGN) website. This 3DPC was georeferenced in the system as ETRS-89 (30N). Firstly, one scenario was registered to the PNOA dataset using the ICP algorithm and considered buildings as stable areas. This process provided a rigid transformation matrix, through an X, Y, and Z translation, along with a *Z*-axis rotation. Both scenarios were georeferenced by applying the same transformation to all the scenarios, using the software CloudCompare [44].

Figure 3. Representative photographs and Remotely Piloted Aircraft Systems images from scenarios A and B (sampling dates: 24 November 2016, and 22 March 2017, respectively).

2.3. Data Analysis

The 3-D models of the two scenarios were compared in order to detect volumetric changes due to erosion/accretion. Both point clouds were rasterized using a pixel size of 0.1 m, and the surface variations were then calculated using two different approaches: (a) height variations using the difference of the coordinates of two rasterized DEMs (Difference of DEMs, henceforth DOD); (b) height variations through the Multiscale Model to Model Cloud Comparison (M3C2) algorithm [45] along a vertical vector. The first approach required the rasterization of the point cloud and was used to calculate the variation of volumes. The second approach could be applied to the raw 3-D point cloud, and it was used to visualize the difference between two scenarios, along with an addressed vector (normal, vertical, or horizontal).

Concerning the volumes calculation, the height difference method determined the method to be used. If the 3-D comparison method was used, the volume variation was calculated as follows. Firstly, for each scenario, a mesh was generated using the Delaunay triangulation or the Poisson reconstruction [46]. Then, the intersection of both meshes was selected, and both were merged into a closed mesh. Then, the volume could be calculated. Alternatively, the 2.5-D comparison could be considered: the two scenarios were rasterized using the same grid size. Both scenarios

were then defined by a first origin point and a grid size in X and Y. Therefore, a point in a scenario had a corresponding point in the second scenario with the same coordinates X and Y. However, each point had its own elevation value or Z value. If the 2.5-D comparison was used, the volume estimation was straightforward. For each point in which there has been a change variation, the volume change associated to that point was equal to the area of the point (i.e., grid size squared) times the height variation. This method eases the discrimination of positive or negative changes.

In addition, volume variations were estimated through a series of representative transects with an equidistant spacing of 10 m and extracted on each scenario (Figure 4). We numbered 1, 3, 5, and 7, since they are selected from the total preliminary transects, which were numbered from 1 to 8 (equidistant spacing of 5 m). Limits between stable areas, sand, seagrass berm, and sea were visually identified on the point cloud using the RGB radiometric information. As the point clouds were georeferenced in the same reference system, the compared transects were overlapped, so no transformation was needed to compare them. Then, an arbitrary level of reference was selected in order to measure the areas of sand. This level must be below the limit of the seagrass berm. The estimation of the sand profile was performed by considering that the dip of the sand profile was constant under the seagrass berm and under the water (based on the schematic profile of banquettes proposed by [7]). Immediately before the seagrass berm, a representative segment of the sand profile was searched, and it was elongated until it intersected the horizontal level of reference. This enabled the measurement of the area of sand in this profile, along with the beach-cast seagrass. Area measurements of sand for each profile enabled the estimation of volumes; the volume assigned to each profile was the measured area multiplied by the separation between transects.

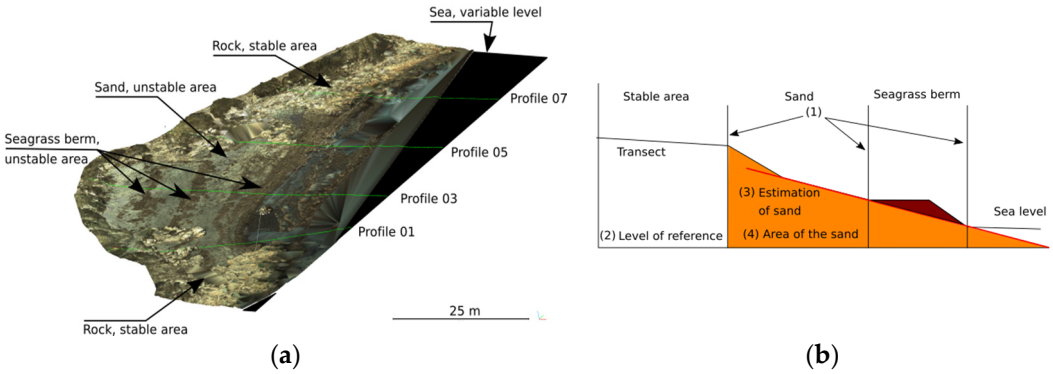

Figure 4. (**a**) Location of the analysed representative profiles; (**b**) Schematic synthesis of the applied methodology to extract the areas through profiles (stable area, sand, and beach-cast seagrass are indicated).

3. Results

To compare both scenarios, the topographical top view and top view of the 3DPC coloured in RGB (Figure 5), the top view of volumetric variation between scenarios (Figure 6), and the representative profile were examined (Figure 7). In scenario A, the distribution of sand had an arch-shaped pattern. In contrast, in scenario B, the sand distribution seemed to be parallel to the coast (Figure 5). In both scenarios, the major part of the litter seagrass deposit was concentrated in a belt with the following proportions: scenario 1: 532 m^2, 7–12 m width; and scenario 2: 906 m^2, 15–23 m width; both with 60 m length.

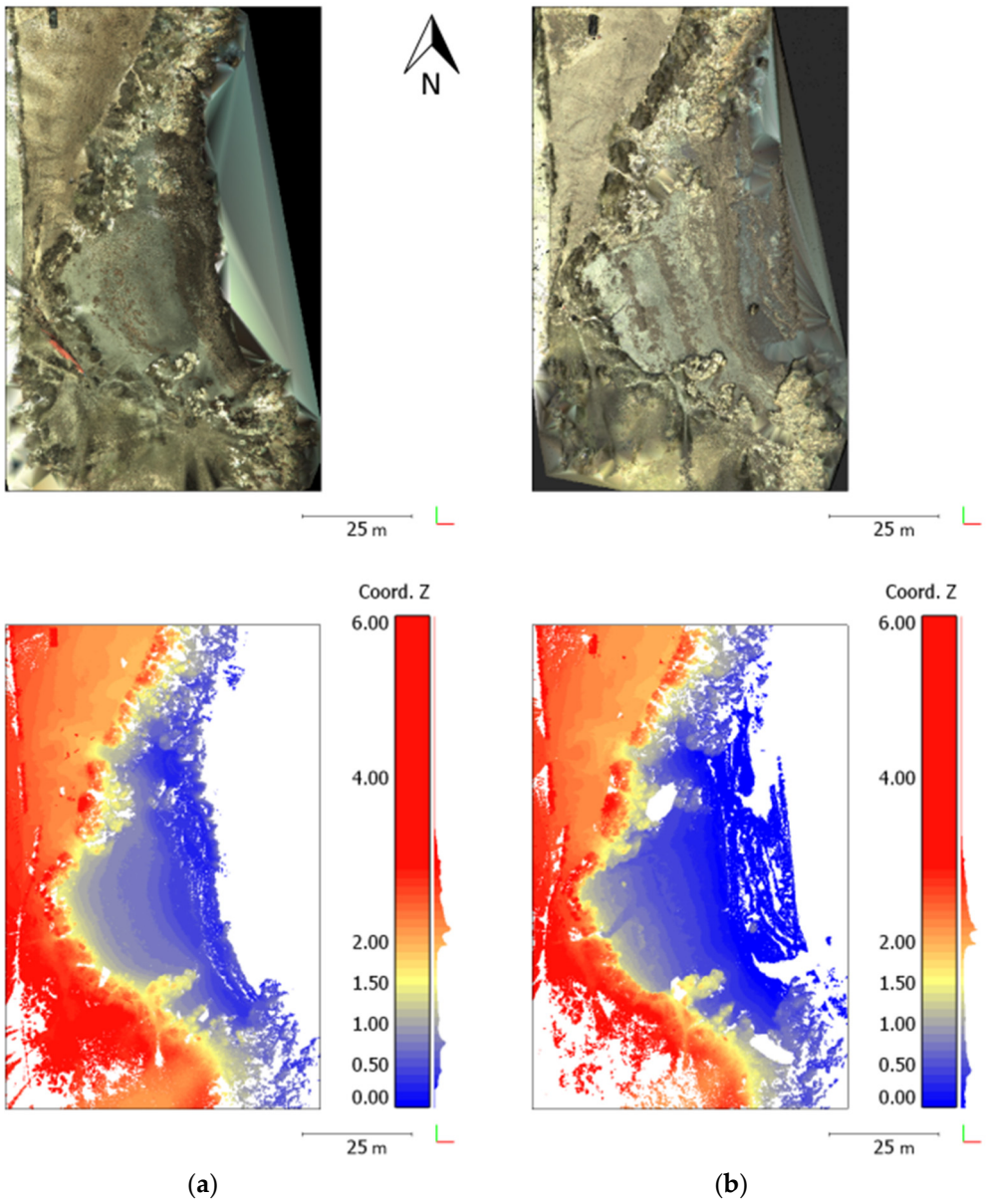

Figure 5. Topographical top view of the 3DPC colored in RGB for the different sampling dates: (**a**) scenario A (mid-autumn): 24 November 2016; (**b**) scenario B (early spring): 22 March 2017.

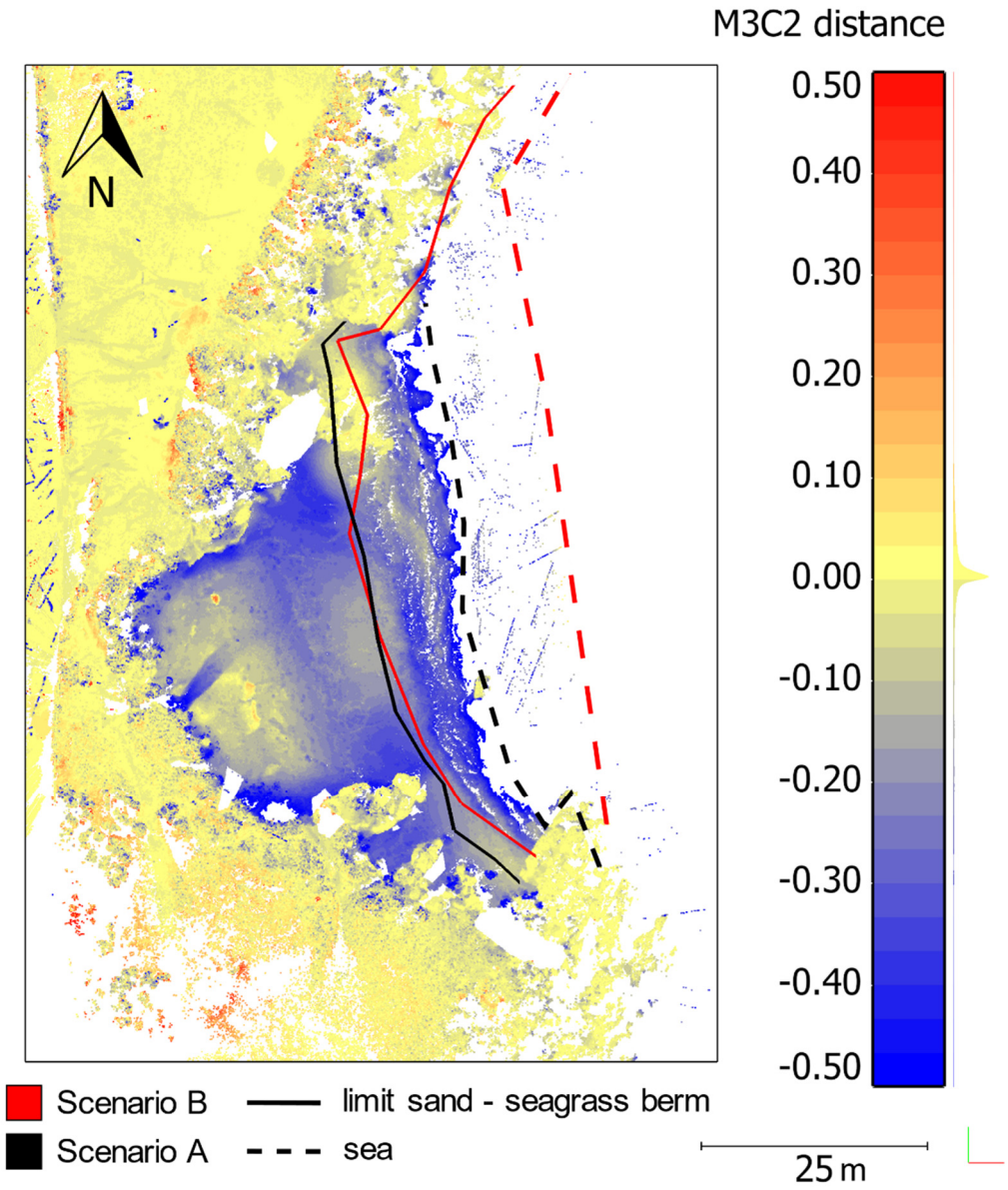

Figure 6. Height variation between scenario/sampling date A: 24 November 2016, and scenario/sampling date B: 22 March 2017. Distances were calculated through the comparison of the respective 3DPC using the Multiscale Model to Model Cloud Comparison (M3C2) in the vertical direction [45]. Negative values show erosion from scenario A to scenario B, while positive values show accretion.

The cross-sectional profiles (Figure 7) reveal a wedge-shaped seagrass berm with maximum heights adjoining the seashore. Scenario A recorded the transition to the summer to winter profile (middle of autumn), where the sand berm was yet be recognized. On the other hand, scenario B (beginning of spring) clearly represented the winter profile, with the typically flatter and more concave beach shape. This last scenario recorded the cumulative loss of sand after several storms recorded in the area.

Our 3-D modelling showed that the peripheral border was the area with high loss of sand, where a storm scarp was developed (Figures 3 and 6). Another important sector with significant erosional change was the generation of a shallow channel due to stormwater runoff (Figures 3 and 6). This channel, located in the middle part of the eastern border of the beach, was up to 1.5 m wide, 0.4 m height, and 5 m long. In scenario B, four different parts of the seagrass berm can be identified: (a) front berm; (b) seagrass berm partially submerged above sea level; (c) two channels located in the extreme of

the beach; and (d) the landward part of the berm, where sand paths could be distinguished. A similar geomorphic "temporary lagoon" within the seagrass berm have been indicated by different authors (e.g., [47]).

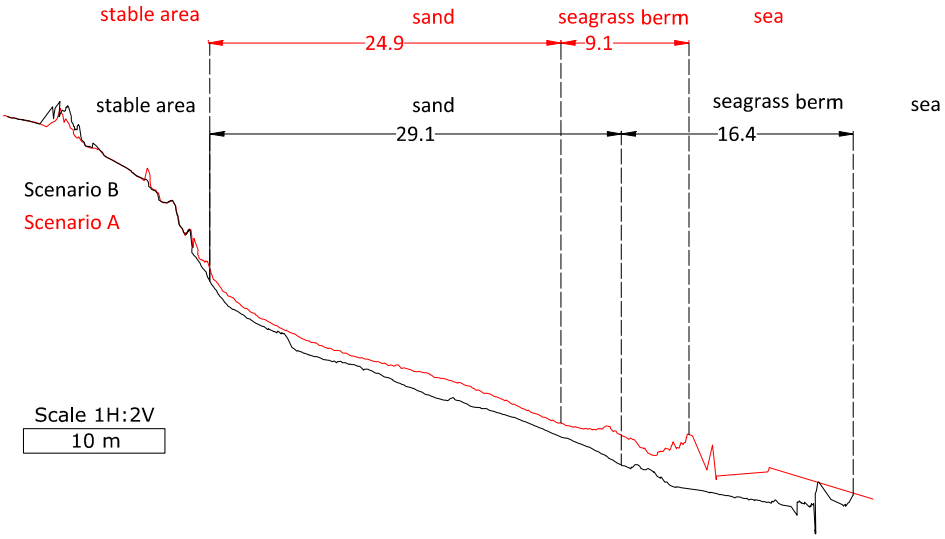

Figure 7. Representative profile number 5 for the two studied scenarios/sampling dates (A: 24 November 2016, and B: 22 March 2017. Note that the vertical scale is twice the horizontal. The limits of the stable area, sand area, and seagrass berm are displayed in the figure.

The volumetric analysis change was based on the data interpolated using five profiles from the LiDAR data cloud (location at Figure 4). As stated before in the methodology section, since the location of the beach-cast seagrass was variable, and the sea level was slightly different in both scenarios, two levels of reference were established. Firstly, the horizontal level, whose position is arbitrary, but the same in both scenarios (Figure 4). Secondly, the beach profile was prolonged (with the same dip) in representative profiles (Figure 8). Therefore, the areal surface of the representative profiles in both scenarios was calculated (Table 1). Consequently, the estimated sand volumetric change was -190.292 m^3.

Table 1. Volumetric change data based on the representative profiles. Four profiles were extracted, and they were separated by 20 m (L). Areas were measured following the procedure shown in Figure 4, with respect to an arbitrary reference level. Zero values mean that no changes were detected in the corresponding profile. Volumes were calculated by multiplying the area measured in the profile by the separation between profiles (L).

Profile	L (m)	Scenario A (m^2)	Scenario B (m^2)	B-A (m^2)	(B-A)xL (m^3)
1	20	39.33	47.13	7.8	156
3	20	63.1601	52.7355	−10.4246	−208.492
5	20	50.46	43.57	−6.89	−137.8
7	20	0	0	0	0
TOTAL					−190.292

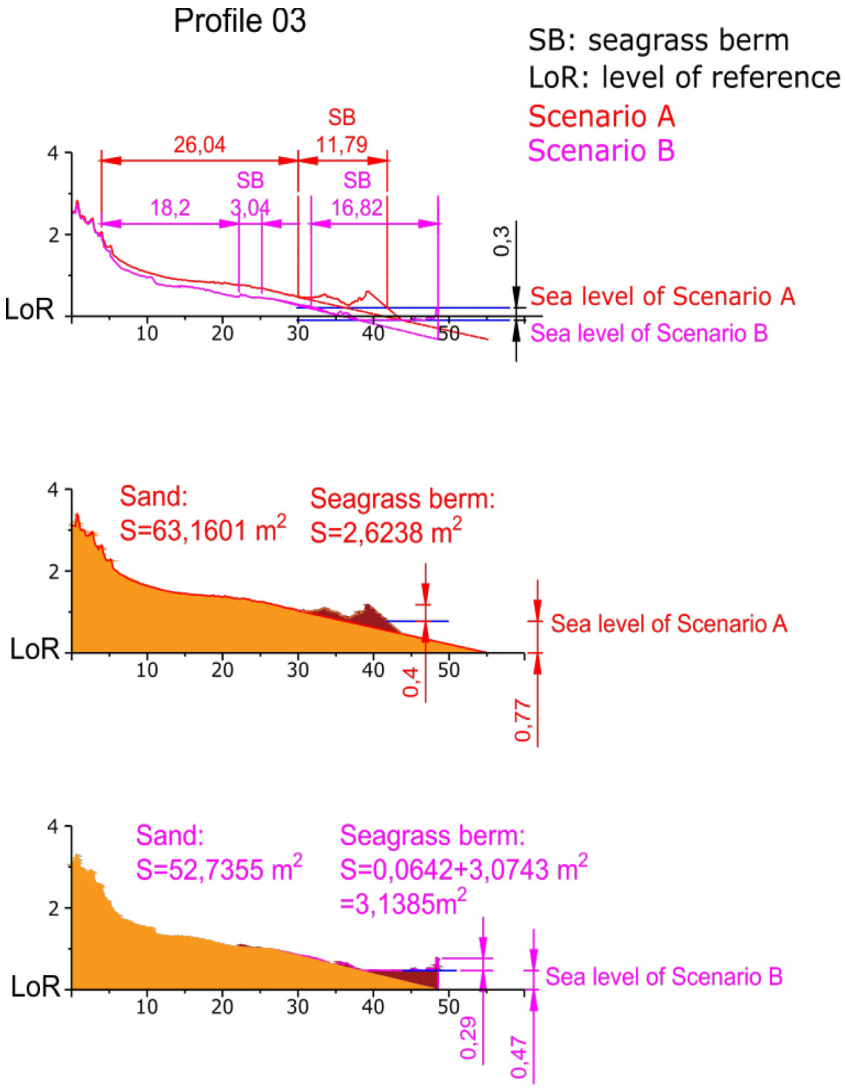

Figure 8. Extraction of areas for profile 3. Front berm height, seagrass berm width, and distance to the stable area are shown.

4. Discussion

A western Mediterranean beach was 3-D modelled with ground based remote sensing techniques (Terrestrial Laser Scanner) in order to develop a novel methodology where high-frequency data acquired at different sampling dates (on time scales ranging from days to months) could be implemented in future studies on a routine basis. We are aware that examining the structure and morphodynamic differences between the two unique scenarios selected are critical since seagrass berms are quite dynamic through time; their structure and position can change on time scales ranging from days to months. For this reason, we contemplated our case study as a methodological proposal, which will be used in future studies of these characteristics beaches.

Previous works used Aerial LiDAR datasets to study the evolution of coastal processes [28,29,48], covering wider areas, but with a lower level of detail than that obtained using TLS instruments. In this work, we used TLS-derived data, which was scanned in high resolution (i.e., separation of points of 5 cm at 100 m). As a number of scans were conducted, their registration provided a high dense point cloud, which was decimated by a separation of points of 1 cm. This high-resolution dataset, which enabled the study of the coastal processes with an unprecedented level of detail, e.g., showing

shallow drainage channels in the sandy beaches (Figure 6) that go unnoticed when using other remote sensing techniques.

One source of error with this method was due to the small angle of incidence of the sensor. As the TLS (model Leica C10 ScanStation) scanned by varying the horizontal and vertical angle, a small angle of incidence of the laser with respect to the sub-horizontal surface implied both (a) a higher horizontal separation between points (and so a lower spatial resolution), and (b) occlusion in some areas as result of a small irregularities of the beach. This error was minimized by considerably increasing the number of scan stations (between 7 and 8 scans per campaign), enabling a high scanning coverage of the beach. It is worth noting that stations could only be performed from the coastal side, and no scan was performed from the other side of the beach, namely the sea. Despite the accuracy of TLS-derived datasets, these issues led to the idea of considering the use of RPAS along with SfM when the use of TLS was not optimal (i.e., very wide areas). Another source of error was found based on the proposed approach, namely the use of transects. Although the variation of volumes using 3-D point clouds could be conducted through the calculation of a closed mesh between scenarios, this calculation would not discriminate the sand from the seagrass berm. As the aim of this work was to estimate the variations of sand, it was considered to separate both. If it was assumed that the dip of the sand tended to be constant, and that the seagrass was deposited on the sand during storms, it was reasonable to consider that the sand and seagrass were separated by the extent of the sand profile (representative profile based on Reference [7]). We were aware that the seagrass berm can also contain sand and silt, although we assumed that can be considered insignificant compared with the total volume of sand lost. Nevertheless, if the changes in volume were in the order class of a magnitude that was much lower, the proposed methodology probably could not be applied. In any case, the use of transects enabled the estimation of the surface of sand with respect to a level of reference. Therefore, the variations of sand could be estimated, but not the total amount of sand on the beach. Multiplying the area of each transect by the separation between transects provided an estimation of the sand's volume. It is worth noting that the more transects that were used, the more accurate the measured estimation. Additionally, the more parallel the profiles were, the lower the error that was obtained.

The use of remote sensing datasets enabled the identification of stable areas, sand, beach-cast seagrass, and sea. Significant height variations were found, especially for sand accumulation. The calculation of height variations was performed through the comparison of high-detail 3-D datasets (more than seven scans were conducted in a 300 m^2 area) using the M3C2 algorithm. Previous works gridded the cloud using a 1 m by 1 m cell [46–48], or 2 m by 2 m [29], and calculated height variations through the Difference of DEMs method (DoD). This process led to a reduction in the definition of such variations. The used methodology, however, enabled the identification of small variations, such as the formation of a drainage channel in the sand.

Height variations could be easily identified, and the estimation of the volume of sand was performed assuming that the sand profile followed a constant dip under the beach-cast seagrass and the sea (Figure 3). Although the bathymetry could be included in this analysis, a simplification was done. A horizontal level of reference was set to close to the sea level. The sand profile was elongated up to this level, such that the sand area for each profile could be estimated. This simplification enabled the comparison of various scenarios with respect to the same level. As a result of this, the variation of sand between scenarios could be calculated.

Previous studies have observed the importance of using high resolution remote sensing techniques to obtain precise beach profiles, and topographic and bathymetric maps (see Reference [26] for a review). In particular, although several studies use LiDAR (mainly airborne) to examine volumetric changes (accretion/erosion) in different sedimentary environments, dunes, or beaches (e.g., [11,28,29,48–52]), a few studies were found that used volumetric estimation (differentiating the sand from the seagrass berm as proposed here) based on Terrestrial LiDAR scanning. Therefore, the straightforward methodology applied in our study case allowed for establishing the

accretion/erosion of sand in a regional area of the Mediterranean coast where the seagrass berm deposit is a common characteristic.

Alicante Province, where our study was performed, presents 244 km of coastline with 91 beaches. This coast experiences a severe pressure of tourist inflow, and several beaches are subject to erosion (example study cases are References [53–57]). Artificial nourishment of beaches is common in this region, notably between 1985 and 1999 [58]. In this sense, the methodology presented here, which enables the estimation of accretion/erosion of sand, can be useful in order to design future management plans along this coast. A further study will focus on the characterization and comparative analysis of the influence of the *Posidonia oceanica* seagrass berms in the sedimentary stability and ecological structuration of the beach. Two beaches will be compared, one subjected to cleaning processes by heavy machinery, and another, which will remain in natural condition without any artificial influence. The obtained results could allow us to estimate the role of the seagrass in the protection of beaches from erosion.

Future works in the studied region, which could use the methodology proposed here, should take into account additional and relevant data in order to establish the detailed morphodynamic evolution trend of these characteristic beaches. In depth examination of the dynamical evolution of these beaches must take into account the following issues: (a) characterization of a number of beach profiles in terms of grain size, total, and foreshore slope; (b) analysis of the long-term coastline evolution in order to verify whether the erosion/accretion trend detected by the LiDAR is in line with the general trend; (c) characterization of the high-frequency morphodynamic evolution, on time scales ranging from hours to days; and (d) characterization of the wave climate through buoy records for at least 10 years in order to identify whether the sediment transport is mainly transverse or longitudinal.

5. Conclusions

Remote sensing datasets provided by TLS devices enabled the monitoring of a pocket beach and the estimation of the variation of sand between different scenarios (-190.292 m^3 in our study) by proposing a straightforward methodology, which discriminates sand and seagrass berm. This work represents the starting point towards developing an accurate monitoring strategy of beaches subjected to erosion, and with characteristic seagrass berm accumulation. Further research will explore the geo-morphodynamic evolution of these beaches throughout the year in order to establish the dynamics of deposition and evolution of the *P. oceanica* seagrass berm in this representative area of south-eastern Spain.

Author Contributions: H.C., A.R., (co-first author) and A.A. conceived, designed, and performed the study. C.M.-B. contributed to the design of the study, data collection, and analysis. All co-authors took part in the writing process.

Funding: This paper was written in the context of the Paleoenvironmental Changes research group (University of Alicante, vigrob-167, Project GR14-05), and partially funded by the University of Alicante (vigrob-157 Project, GRE14-04, GRE14-05 and GRE15-19 Projects), the Spanish Ministry of Economy and Competitiveness (MINECO) and EU FEDER, under Projects TIN2014-55413-C2-2-P and TEC2017-85244-C2-1-P.

Acknowledgments: The authors would like to thank Alfonso Ramos, coordinator and scientific director of the Marine Research Centre in Santa Pola, CIMAR, University of Alicante, for his continuous support in this research. Thanks to Andres Izquierdo, José M. González Correa, and Santa Pola Council. Thanks are given to anonymous reviewers for their valuable comments on our manuscript.

Conflicts of Interest: The authors declare no conflict of interest.

References

1. Short, A.D. The role of wave height, period, slope, tide range and embaymentisation in beach classifications: A review. *Rev. Chil. Hist. Nat.* **1996**, *69*, 589–604.
2. Robertson, A.I.; Lenanton, R.C.J. Fish community structure and food chain dynamics in the surf-zone of sandy beaches: The role of detached macrophyte detritus. *J. Exp. Mar. Biol. Ecol.* **1984**, *84*, 265–283. [CrossRef]

3. Lenanton, R.C.J.; Robertson, A.I.; Hansen, J.A. Nearshore accumulations of detached macrophytes as nursery areas for fish. *Mar. Ecol. Prog. Ser.* **1984**, *9*, 51–57. [CrossRef]
4. Van der Merwe, D.; McLachlan, A. Significance of free-floating macrophytes in the ecology of a sandy beach surf zone. *Mar. Ecol. Prog. Ser.* **1987**, *38*, 53–63. [CrossRef]
5. Orr, K.K.; Wilding, T.A.; Horstmeyer, L.; Weigl, S.; Heymans, J.J. Detached macroalgae: Its importance to inshore sandy beach fauna. *Estuar. Coast. Shelf Sci.* **2014**, *150*, 125–135. [CrossRef]
6. Boudouresque, C.F.; Meinesz, A. *Découverte de L'herbier de Posidonies*; Cahiers Parc National de Port-Cros: Gardanne, France, 1982.
7. Simeone, S.; De Falco, G. Posidonia oceanica banquette removal: Sedimentological, geomorphological and ecological implications. *J. Coast. Res.* **2013**, *65*, 1045–1050. [CrossRef]
8. Ochieng, C.A.; Erftemeijer, P.L. Accumulation of seagrass beach cast along the Kenyan coast: A quantitative assessment. *Aquat. Bot.* **1999**, *65*, 221–238. [CrossRef]
9. Boudouresque, C.F.; Jeudy de Grissac, A. L'herbier à Posidonia oceanica en Méditerranée: Les interactions entre la plante et le sédiment. *J. Rech. Océanogr.* **1983**, *8*, 99–122.
10. Jeudy de Grissac, A. Effets des herbiers à Posidonia oceanica sur la dynamique marine et la sedimentology littorale. In *International Workshop on Posidonia oceanica Meadows*; Boudouresque, C.F., Jeudy de Grissac, A., Oliver, J., Eds.; GIS Posidonie Publisher: Marseille, France, 1984; pp. 437–443.
11. Simeone, S.; De Falco, G. Morphology and composition of beach-cast *Posidonia oceanica* litter on beaches with different exposures. *Geomorphology* **2012**, *151*, 224–233. [CrossRef]
12. Ros, J.; Romero, J.; Ballesteros, E.; Gili, J.M. Diving in Blue Water. The Benthos. In *Western Mediterranean*; Margalef, R., Ed.; Pergamon Press: London, UK, 1985; pp. 233–295.
13. Vacchi, M.; De Falco, G.; Simeone, S.; Montefalcone, M.; Morri, C.; Ferrari, M.; Bianchi, C.N. Biogeomorphology of the Mediterranean *Posidonia oceanica* seagrass meadows. *Earth Surf. Process. Landf.* **2016**, *42*, 243–386. [CrossRef]
14. Mas, J.; Franco, I.; Demestre, M.; Guillén, J.; Murcia, F.J.; Ruiz, J.M. Benthic communities on shallow sedimentary bottoms in the Western Mediterranean. In *Atlas of Bedforms in the Western Mediterranean*; Guillén, J., Acosta, J., Latino-Chiocci, F., Palanques, A., Eds.; Springer: Basel, Switzerland, 2017; pp. 199–206.
15. Mateo, M.A.; Sánchez-Lizaso, J.L.; Romero, J. *Posidonia oceanica* 'banquettes': A preliminary assessment of the relevance for meadow carbon and nutrients budget. *Estuar. Coast. Shelf Sci.* **2003**, *56*, 85–90. [CrossRef]
16. Gómez-Pujol, L.; Orfila, A.; Álvarez-Ellacuría, A.; Terrado, J.; Tintoré, J. *Posidonia oceanica* beach-cast litter in Mediterranean beaches: A coastal videomonitoring study. *J. Coast. Res.* **2013**, *65*, 1768–1773. [CrossRef]
17. Romero, J.; Pergent, G.; Martini, C.; Mateo, M.A.; Regnier, C. The detritic compartment in a *Posidonia oceanica* meadow: Litter features, decomposition rates, and mineral stocks. *Mar. Ecol.* **1992**, *13*, 69–83. [CrossRef]
18. Ferrandis, E.; Bartolomé, F. Dulces bárbaros del Este y del Oeste (Análisis estadístico de los vientos en la bahía de Alicante). In *La Reserva Marina de la Isla Plana o Nueva Tabarca (Alicante)*, 1st ed.; Ramos-Esplá, A.A., Ed.; Ayuntamiento de Alicante, Universidad de Alicante: Alacant, Spain, 1985; pp. 51–94.
19. De Falco, G.; Simeone, S.; Baroli, M. Management of beach-cast *Posidonia oceanica* seagrass on the island of Sardinia (Italy, Western Mediterranean). *J. Coast. Res.* **2008**, *24*, 69–75. [CrossRef]
20. Brock, J.C.; Purkis, S.J. The emerging role of lidar remote sensing in coastal research and resource management. *J. Coast. Res.* **2009**, *53*, 1–5. [CrossRef]
21. Johnson, K.M.; Ouimet, W.B. Rediscovering the lost archaeological landscape of southern New England using airborne light detection and ranging (LiDAR). *J. Archaeol. Sci.* **2014**, *43*, 9–20. [CrossRef]
22. Chiabrando, F.; Spanò, A.; Sammartano, G.; Teppati Losè, L. UAV oblique photogrammetry and lidar data acquisition for 3D documentation of the Hercules Fountain. *Virtual Archaeol. Rev.* **2017**, *8*, 83. [CrossRef]
23. Luo, S.; Wang, C.; Xi, X.; Pan, F.; Peng, D.; Zou, J.; Nie, S.; Qin, H. Fusion of airborne LiDAR data and hyperspectral imagery for aboveground and belowground forest biomass estimation. *Ecol. Indic.* **2017**, *73*, 378–387. [CrossRef]
24. Westoby, M.J.; Brasington, J.; Glasser, N.F.; Hambrey, M.J.; Reynolds, J.M. 'Structure-from-Motion' photogrammetry: A low-cost, effective tool for geoscience applications. *Geomorphology* **2012**, *179*, 300–314. [CrossRef]
25. Riquelme, A.; Cano, M.; Tomás, R.; Abellán, A. Identification of rock slope discontinuity sets from laser scanner and photogrammetric point clouds: A comparative analysis. *Procedia Eng.* **2017**, *191*, 838–845. [CrossRef]

26. Klemas, V. Beach profiling and LIDAR bathymetry: An overview with case studies. *J. Coast. Res.* **2011**, *27*, 1019–1028. [CrossRef]
27. Andrews, B.D.; Gares, P.; Colby, J.D. Techniques for GIS modeling of coastal dunes. *Geomorphology* **2002**, *48*, 289–308. [CrossRef]
28. Woolard, J.W.; Colby, J.D. Spatial characterization, resolution, and volumetric change of coastal dunes using airborne LIDAR: Cape Hatteras, North Carolina. *Geomorphology* **2002**, *48*, 269–287. [CrossRef]
29. Saye, S.E.; Van der Wal, D.; Pye, K.; Blott, S.J. Beach–dune morphological relationships and erosion/accretion: An investigation at five sites in England and Wales using LIDAR data. *Geomorphology* **2005**, *72*, 128–155. [CrossRef]
30. Lorenzo-Lacruz, J.; Pons, G.X.; Mir-Gual, M. Mapeo semi-automatizado de campos de dunas mediante tecnología LIDAR: Aplicación en el sistema dunar de Sa Canova de Artá (Mallorca). *IX Jornadas de Geomorfología Litoral* **2017**, *17*, 135–138.
31. Sallenger, A.H., Jr.; Krabill, W.B.; Swift, R.N.; Brock, J.; List, J.; Hansen, M.; Holmas, R.A.; Manizade, S.; Sontag, J.; Meredith, A.; et al. Evaluation of airborne topographic lidar for quantifying beach changes. *J. Coast. Res.* **2003**, *19*, 125–133.
32. Gares, P.A.; Wang, Y.; White, S.A. Using LIDAR to monitor a beach nourishment project at Wrightsville Beach, North Carolina, USA. *J. Coast. Res.* **2006**, *22*, 1206–1219. [CrossRef]
33. Nicoletti, L.; Valentini, E.; Targusi, M.; La Valle, P.; Fornari, A.; Taramelli, A. Characterisation of *Posidonia oceanica* meadows using both hyperspectral and LIDAR data: A new approach. *Biol. Mar. Mediterr.* **2010**, *17*, 173–174.
34. Simeone, S.; De Muro, S.; De Falco, G. Seagrass berm deposition on a Mediterranean embayed beach. *Estuar. Coast. Shelf Sci.* **2013**, *135*, 171–181. [CrossRef]
35. Simeone, S.; De Falco, G.; Quattrocchi, G.; Cucco, A. Morphological changes of a Mediterranean beach over one year (San Giovanni Sinis, western Mediterranean). *J. Coast. Res.* **2014**, *70*, 217–222. [CrossRef]
36. González-Correa, J.M.; Torquemada, Y.F.; Lizaso, J.L.S. Long-term effect of beach replenishment on natural recovery of shallow Posidonia oceanica meadows. *Estuar. Coast. Shelf Sci.* **2007**, *76*, 834–844. [CrossRef]
37. Olcina-Cantos, J.; Torres-Alfosea, F.J. Incidencia de los temporales de levante en la ordenación del litoral alicantino. *Papeles de Geografía* **1997**, *26*, 109–136.
38. López, I.; Aragonés, L.; Villacampa, Y. Analysis and modelling of cross-shore profile of gravel beaches in the province of Alicante. *Ocean Eng.* **2016**, *118*, 173–186. [CrossRef]
39. Carrea, D.; Abellán, A.; Humair, F.; Matasci, B.; Derron, M.H.; Jaboyedoff, M. Correction of terrestrial LiDAR intensity channel using Oren–Nayar reflectance model: An application to lithological differentiation. *J. Photogramm. Remote Sens.* **2016**, *113*, 17–29. [CrossRef]
40. Leica Geosystems AG. *Leica ScanStation C10 Data Sheet*; Leica Geosystems AG: Heerbrugg, Switzerland, 2011.
41. Besl, P.J.; McKay, N.D. A method for registration of 3-D shapes. *IEEE Trans. Pattern Anal. Mach. Intell.* **1992**, *14*, 239–256. [CrossRef]
42. James, M.R.; Robson, S.; d'Oleire-Oltmanns, S.; Niethammer, U. Optimising UAV topographic surveys processed with structure-from-motion: Ground control quality, quantity and bundle adjustment. *Geomorphology* **2017**, *280*, 51–66. [CrossRef]
43. Leica. Cyclone v9.1. Leica Geosystems. 2016. Available online: http://leica-geosystems.com/products/laser-scanners/software/leica-cyclone (accessed on 24 November 2017).
44. CloudCompare (Version 2.8) [GPL Software]. 2018. Available online: http://www.cloudcompare.org/ (accessed on 19 June 2018).
45. Brodu, N.; Lague, D. 3D point cloud classification of complex natural scenes using a multi-scale dimensionality criterion: Applications in geomorphology. *J. Photogramm. Remote Sens.* **2012**, *68*, 121–134. [CrossRef]
46. Lai, P.; Samson, C.; Bose, P. Visual enhancement of 3D images of rock faces for fracture mapping. *Int. J. Rock Mech. Min. Sci.* **2014**, *72*, 325–335. [CrossRef]
47. Boudoresque, C.F.; Ponel, P.; Astruch, P.; Barcelo, A.; Blanfuné, A.; Geoffroy, D.; Thibaut, T. The high heritage value of the Mediterranean sandy beaches, with a particular focus on the *Posidonia oceanica* "banquettes": A review. *Sci. Rep. Port-Cros Natl. Park* **2017**, *31*, 23–70.
48. Burvingt, O.; Masselink, G.; Russell, P.; Scott, T. Beach response to consecutive extreme storms using LiDAR along the SW coast of England. *J. Coast. Res.* **2016**, *75*, 1052–1056. [CrossRef]

49. Pietro, L.S.; O'neal, M.A.; Puleo, J.A. Developing terrestrial-LIDAR-based digital elevation models for monitoring beach nourishment performance. *J. Coast. Res.* **2008**, *24*, 1555–1564. [CrossRef]
50. Zhou, G. Coastal 3D change pattern analysis using LIDAR series data. In *Remote Sensing of Coastal Environments*; Wang, Y., Ed.; CRC Press: Boca Raton, FL, USA, 2010; pp. 103–120.
51. Stockdonf, H.F.; Sallenger, A.H., Jr.; List, J.H.; Holman, R.A. Estimation of shoreline position and change using airborne topographic lidar data. *J. Coast. Res.* **2002**, *18*, 502–513.
52. Young, A.P.; Ashford, S.A. Application of airborne LIDAR for seacliff volumetric change and beach-sediment budget contributions. *J. Coast. Res.* **2006**, *22*, 307–318. [CrossRef]
53. Aragonés, L.; García-Barba, J.; García-Bleda, E.; López, I.; Serra, J. Beach nourishment impact on *Posidonia oceanica*: Case study of Poniente Beach (Benidorm, Spain). *Ocean Eng.* **2015**, *107*, 1–12. [CrossRef]
54. López, I.M.; López, M.; Aragonés, L.; Garcia-Barba, J.; López, M.P.; Sánchez, I. The erosion of the beaches on the coast of Alicante: Study of the mechanisms of weathering by accelerated laboratory tests. *Sci. Total Environ.* **2016**, *566*, 191–204. [CrossRef] [PubMed]
55. Pagán, J.I.; Aragonés, L.; Tenza-Abril, A.J.; Pallarés, P. The influence of anthropic actions on the evolution of an urban beach: Case study of Marineta Cassiana Beach, Spain. *Sci. Total Environ.* **2016**, *559*, 242–255. [CrossRef] [PubMed]
56. Pagán, J.I.; López, M.; López, I.; Tenza-Abril, A.J.; Aragonés, L. Causes of the different behaviour of the shoreline on beaches with similar characteristics. Study case of the San Juan and Guardamar del Segura beaches, Spain. *Sci. Total Environ.* **2018**, *634*, 739–748. [CrossRef] [PubMed]
57. Chiva, L.M.; Pagán, J.I.; López, I.; Tenza-Abril, A.J.; Aragonés, L.; Sánchez, I. The effects of sediment used in beach nourishment: Study case El Portet de Moraira beach. *Sci. Total Environ.* **2018**, *628*, 64–73. [CrossRef] [PubMed]
58. Beachmed. *Evaluación de Recursos Sedimentarios en Los Fondos Antelitorales de la Comunidad Valenciana*; Generalitat Valenciana: Valencia, Spain, 2003.